The Journal of Neuroscience, October 15, 2002, 22(20):9053–9062

Bursting Neurons Signal Input Slope

Adam Kepecs, Xiao-Jing Wang, and John Lisman

Volen Center for Complex Systems, Brandeis University, Waltham, Massachusetts 02454

Brief bursts of high-frequency action potentials represent a common firing mode of pyramidal neurons, and there are indications that they represent a special neural code. It is therefore of interest to determine whether there are particular spatial and temporal features of neuronal inputs that trigger bursts. Recent work on pyramidal cells indicates that bursts can be initiated by a specific spatial arrangement of inputs in which there is coincident proximal and distal dendritic excitation (Larkum et al., 1999). Here we have used a computational model of an important class of bursting neurons to investigate whether there are special temporal features of inputs that trigger bursts. We find that when a model pyramidal neuron receives sinusoidally or randomly varying inputs, bursts occur preferentially on the positive slope of the input signal. We further find that the number of spikes per burst can signal the magnitude of the slope in a graded manner. We show how these computations can be understood in terms of the biophysical mechanism of burst generation. There are several examples in the literature suggesting that bursts indeed occur preferentially on positive slopes (Guido et al., 1992; Gabbiani et al., 1996). Our results suggest that this selectivity could be a simple consequence of the biophysics of burst generation. Our observations also raise the possibility that neurons use a burst duration code useful for rapid information transmission. This possibility could be further examined experimentally by looking for correlations between burst duration and stimulus variables.

Key words: burst; biophysical model; pyramidal cell; weakly electric fish; ELL; neural coding; simulation

A fundamental aspect of neuronal function is how the output spike pattern of a neuron is determined by its synaptic input. A simple and highly successful formulation of this process has been the "integrate-and-fire" model (Lapicque, 1907). According to this model, neurons integrate synaptic input via their membrane capacitance and fire spikes when their voltage reaches spike threshold (Lapicque, 1907; Tuckwell, 1988). For the many types of neurons that obey this principle, the rate of spiking directly reflects the amplitude of the input current (Kistler et al., 1997; Binder et al., 1999).

However, many neurons possess additional voltage-gated conductances that can participate in the generation of more complex firing patterns. For instance, intrinsic conductances can generate brief, high-frequency bursts of action potentials that are commonly observed in recordings from a variety of brain regions (Kandel and Spencer, 1961; Barker and Gainer, 1975; King et al., 1976; Cattaneo et al., 1981a; Eisen and Marder, 1982; Gariano and Groves, 1988; Reinagel et al., 1999; Martinez-Conde et al., 2000; Ramcharan et al., 2000). There is evidence that such bursts represent a special neural code (Gabbiani et al., 1996; Lisman, 1997; Sherman, 2001). For instance, hippocampal place-fields are more accurately defined (Otto et al., 1991; Molden et al., 2001) (but see Harris et al., 2001), feature selectivity of some neurons in the visual cortex is sharpened (Cattaneo et al., 1981b; Livingstone et al., 1996), and feature extraction by electric fish pyramidal cells is more reliable (Gabbiani et al., 1996) when only spikes belonging to bursts are considered. In monkeys performing a motion discrimination task, the burst rate was found to reflect the direction of visual stimulus better than the average firing rate (Bair et al., 1994). *In vitro*, bursts of pyramidal neurons were found to underlie population synchrony in the cortex (Silva et al., 1991) and the hippocampus (Miles et al., 1988). Bursting has been shown to play crucial roles in synaptic plasticity both presynaptically (Pavlides et al., 1988; Huerta and Lisman, 1995) as well as postsynaptically (Thomas et al., 1998; Pike et al., 1999). Furthermore, some forms of short-term plasticity allow synapses to reliably transmit bursts but filter out single spikes (Lisman, 1997; Matveev and Wang, 2000). Given this evidence for the importance of bursts, it is crucial to understand which properties of neuronal input trigger burst firing.

We have examined this issue using a computational model of a common class of bursting neurons. We stimulated the model with sinusoidal and random current input and looked for the temporal input features that trigger bursts. Our main conclusion is that the membrane conductances that generate bursts can make the neuronal output dependent more on the slope of the input current than its amplitude. This result may explain previous experimental observations that some bursting neurons are involved in the behaviorally important process of detecting the slope of sensory signals (Gabbiani et al., 1996; Metzner et al., 1998; Sherman, 2001). Our work also revealed a novel aspect of burst-mediated signaling: the magnitude of the slope can be encoded by the number of spikes per burst. Because burst duration could transmit graded information in <20 msec, it may be an especially useful coding mechanism when rapid information transmission is at a premium.

MATERIALS AND METHODS

Neuron model. We used a model neuron that includes only the minimal biophysical mechanisms necessary to reproduce bursting in a pyramidal cell (Traub et al., 1991; Pinsky and Rinzel, 1994; Kamondi et al., 1998;

Received Jan. 30, 2002; revised July 16, 2002; accepted July 24, 2002.

This work was supported by grants from the National Institutes of Health, W. M. Keck Foundation, and the Alfred P. Sloan Foundation. We thank Larry Abbott, Eve Marder, and Sridhar Raghavachari for comments on a previous version of this manuscript and Jeremy Caplan, Enrique Garibay, and Sridhar Raghavachari for useful discussions.

Correspondence should be addressed to Xiao-Jing Wang, Volen Center for Complex Systems, MS 013, Brandeis University, 415 South Street, Waltham, MA 02454-9110. E-mail: xjwang@brandeis.edu.

Mainen and Sejnowski, 1996; Doiron et al., 2001). We represent the soma and the axon lumped into one compartment containing the channels necessary for spike generation (I_{Na} and I_K), which result in a type I membrane (Hodgkin, 1948; Rinzel and Ermentrout, 1989; Wang and Rinzel, 1995; Wang and Buzsáki, 1996). The dendritic compartment includes a slowly activating potassium, I_{KS}, and a persistent sodium, I_{NaP}, current (Azouz et al., 1996), which together are responsible for burst generation. The membrane potential obeys the following equations (Kamondi et al., 1998): $C_m dV_s/dt = -I_{Na} - I_K - I_{leak} - g_c(V_s - V_d)/p + I_{soma}$ and $C_m dV_d/dt = -I_{NaP} - I_{KS} - I_{Leak} - g_c(V_d - V_s)/(1 - p) + I_{dendrite}$. The voltage-dependent conductances are described using standard Hodgkin–Huxley formalism. The kinetics of a gating variable x are described by $dx/dt = \phi_x(\alpha_x(1 - x) - \beta_x x) = \phi_x(x_\infty - x)/\tau_x$. $I_{Na} = g_{Na} m_\infty^3 h(V - E_{Na})$, where $m_\infty = \alpha_m/(\alpha_m + \beta_m)$, $\alpha_m = -0.1(V + 31)/(\exp(-0.1(V + 31)) - 1)$, $\beta_m = 4\exp(-(V + 56)/18)$; $\alpha_h = 0.07\exp(-(V + 47)/20)$, and $\beta_h = 1/\exp(-0.1(V + 17)) + 1)$. $I_K = g_K n^4(V - E_K)$, where $\alpha_n = -0.01(V + 34)/(\exp(-0.1(V + 34)) - 1)$, and $\beta_n = 0.125(-(V + 44)/80)$. $I_{NaP} = g_{NaP} T_\infty^3(V - E_{Na})$, $r_\infty(V) = 1/(1 + (-(V + 57.7)/7.7))$. $I_{KS} = g_{KS} q(V - E_K)$, where $q_\infty(V) = 1/(1 + \exp(-(V + 35)/6.5))$ and $\tau_q(V) = \tau q0/(\exp(-(V + 55)/30) + \exp((V + 55)/30))$. $I_{Leak} = g_{Leak}(V - E_{Leak})$, $C_m = 1\ \mu F/cm^2$. The coupling conductance between compartments is $g_c = 1\ mS/cm^2$. In Figures 2*a*, 3*b,* and 6, *a* and *b*, we only use the somatic compartment, $g_c = 0$, whereas in Figure 2*d* we obtain adaptation by setting $g_c = 0.1$. The asymmetry between the areas of the two compartments is taken into account in the parameter p = somatic area/total area = 0.15. The total membrane area is assumed to be 60,000 μm^2. The temperature scaling factors are $\phi_h = \phi_n = 3.33$. Other parameter values are: $g_{Leak} = 0.18$, $g_{Na} = 45$, $g_K = 20$, $g_{NaP} = 0.12$, and $g_{KS} = 0.8$ in mS/cm^2. In some simulations we modified the bursting conductances $g_{NaP} = 0.09$, $g_{KS} = 0.9$ to obtain intermixed bursts and spikes. The activation time constant of I_{KS} is scaled by τ_{q0}, which was set to 200 msec unless otherwise noted (see Fig. 3*e*). The ionic reversal potentials are $E_{Leak} = -65$, $E_{Na} = +55$, and $E_K = -90$ in mV. Numerical integration was performed with a fourth-order Runge–Kutta method using a 0.01 msec time step. Bifurcation analysis was done using AUTO (Doedel, 1981) in XPP (Ermentrout, 2002).

We simulated two other models that differ in the specific ionic mechanisms of burst generation but belong the same broad class of bursters. One model is based on a calcium-dependent bursting mechanism (Wong et al., 1979; Traub et al., 1991). In this model the dendritic compartment contains a high-threshold calcium current, I_{CaL}, and a calcium-dependent potassium current, I_{AHP}. The parameters are the same as in Wang (1998), except $g_{Ca} = 0.35$, $g_{AHP} = 6.5$, $g_c = 1.5$ (in mS/cm^2), and $p = 0.2$. Another model tested is the chattering cell model as in Wang (1999), except $g_{NaP} = 0.09$ and $g_{KS} = 10.0$. Simulation code for these models can be found at http://www.bio.brandeis.edu/lismanlab/bursting/.

Stimulus generation. We generated random stimuli in the frequency domain with a flat power spectrum up to a given cutoff frequency, f_c. The cutoff frequency introduces correlations in the input at $\tau_{corr} = 1/2f_c$. For instance, in Figure 4 the use of $f_c = 5$ Hz creates correlations at the time scale of 100 msec.

Spike train analysis. The spike trains in response to random current injections were segmented into bursts and single spikes based on an interspike interval (ISI) threshold. Bursts were defined as the set of spikes occurring within 10 msec of another spike. This ISI threshold was based on the ISI distribution, but small changes did not affect the qualitative results.

Signal detection theory. We characterized the differences between the coding properties of different bursts using the receiver-operating characteristic (ROC) (Green and Swets, 1966). We use ROC analysis to characterize how well certain aspects of the stimulus predict the burst output. This in turn allows us to evaluate how bursts of different durations signal different aspects of the stimulus. The ROC curve characterizes the range of decision options available for different detection criteria. For any set rate of false alarms, P_{FA}, the probability of correct detection, P_D, is plotted. The diagonal, $P_{FA} = P_D$, represents chance level detection. The more bowed a curve toward the top-left corner, the better the overall detectability.

The discriminability index is defined as the area under the ROC curve, signifying the probability of correct discrimination (Gabbiani and Koch, 1998). The discriminability between 2 and 3 spike bursts is defined as $P_{D:\,2-3} = \int_{-\infty}^{\infty} P(B2 = x)\, P(B3 < x)\, dx$, where *B2* and *B3* denote two and three spikes bursts, respectively, and x is either the amplitude or the slope of the input. $P(B2 = x)$ represents the probability that a two-spike burst occurs at x, whereas $P(B3 < x)$ represents the probability that a burst of three spikes will occur below x. Here, x can represent any aspect of the stimulus, and we used either the amplitude or the slope of the current.

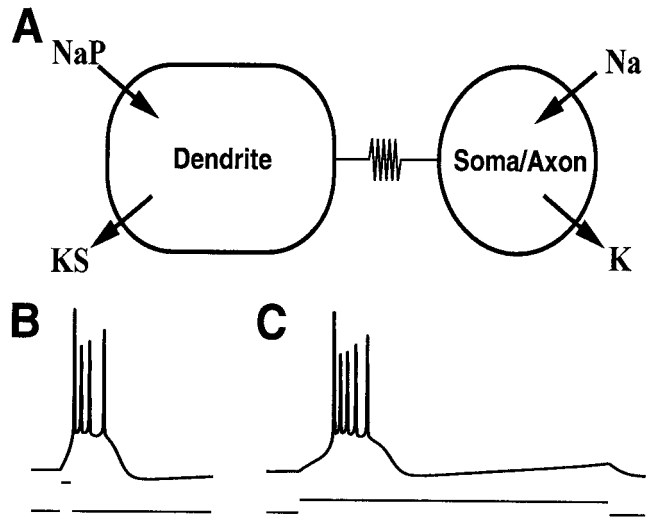

Figure 1. Model of a bursting neuron. *A,* Two-compartment model of pyramidal neurons. The somatic region contains Hodgkin–Huxley-type currents that generate fast spikes, and the dendrite contains a persistent sodium and a slow potassium current responsible for bursting. *B,* A brief current injection to the dendritic compartment induces a burst that outlasts the stimulus. This is a form of fast positive feedback. *C,* Burst firing terminates even for a sustained current injection. This is indicative of a negative feedback process. The current pulse is 6 msec in *B* and 225 msec in *C*.

RESULTS

To investigate the signaling properties of bursts we used a standard model of bursting pyramidal neurons (Fig. 1*A*) (Traub et al., 1991; Rhodes and Gray, 1994; Pinsky and Rinzel, 1994; Mainen and Sejnowski, 1996; Kamondi et al., 1998; Wang, 1999; Kepecs and Wang, 2000; Doiron et al., 2001). This model captures the general features of burst generation in pyramidal cells, in particular the interaction of the soma and the dendrites in burst generation (Wong et al., 1979; Turner et al., 1994; Hoffman et al., 1997; Golding et al., 1999; Williams and Stuart, 1999). The soma contains the classic Hodgkin–Huxley currents responsible for spike generation (a Na^+ current with fast inactivation and a K^+ current). The dendrite contains the currents responsible for bursting: a fast-activating, persistent inward current, I_{NaP}, and a slowly activating potassium current, I_{KS} (Fig. 1*A*). The role of the persistent inward current is to produce a regenerative current that drives the high firing rate (100–300 Hz) during a burst. Because the inward current is regenerative, a burst can outlast the brief inward current that triggers it (Fig. 1*B*). On the other hand, bursts terminate abruptly because of the slowly activating K^+ current, even when the input is sustained (Fig. 1*C*). These two properties are characteristic of a broad class of bursting neurons. This model is just one implementation of the many possible ionic mechanisms for bursting that can be characterized by a fast positive feedback process (underlying Fig. 1*B*) coupled to slower negative feedback (underlying Fig. 1*C*).

Slope detection by bursts

Using this model we examined how the temporal properties of the neuronal input affect burst initiation. A traditional Hodgkin–Huxley neuron fires at a rate proportional to the input amplitude and thus fires symmetrically on both rising and falling phases of

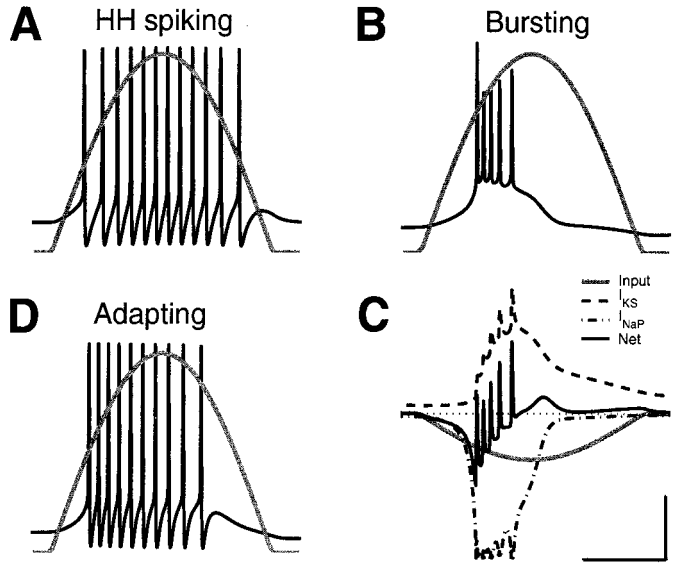

Figure 2. Biophysics of bursts leads to detection of the up-stroke of 4 Hz current stimulus. *A,* Tonically spiking neuron. With only spiking currents (I_{HH}) the firing in response to a sinusoid current is symmetric with respect to the peak of the input current. *B,* Bursting neuron. Bursts occur on the rising edge of the sinusoidal input. *C,* Mechanism of slope selectivity. After the burst is terminated, the slow I_{KS} remains elevated and counteracts the input current, so that the net current flow is almost zero (*dotted line* represents 0 current). Calibration: 4 nA, 50 msec. *D,* Adapting neuron. Adaptation only weakly breaks the firing symmetry.

a 4 Hz sinusoidal input (Fig. 2*A*). In contrast, if the conductances that produce bursting are present, the cell fires bursts exclusively on the rising phase of the 4 Hz signal (Fig. 2*B*). These results gave the first indication that bursting neurons signal positive slope. Examination of the individual conductances provides insight into how selectivity to upstrokes is achieved: each spike of the burst produces a cumulative elevation of the slow dendritic potassium current, I_{KS} (Fig. 2*C*). This enhanced K^+ current eventually terminates the burst and, because it turns off slowly, prevents firing on the falling phase of the input. It is these hysteretic properties that break the firing symmetry. Note that spike frequency adaptation produced by I_{KS} alone could break the symmetry (Fig. 2*D*). However, the bursting that is generated when a fast inward current is also present provides a very strong form of adaptation (Fig. 1*C*), enhancing slope detection. Without this inward current (fast positive feedback) the firing rate on the rising edge is low so there is little negative feedback and hence the difference between the rates on the rising and falling phases is not large. Additionally, the fast inward current produces the high spike rates that contribute to coding, as will be discussed later.

If bursting neurons are robust slope detectors, this capability should not be restricted to sinusoidal inputs. We therefore examined the behavior of the model with random input signals (Fig. 3*A*). Our simulations showed that spikes within bursts occurred preferentially on the positive slopes of stimuli, whereas isolated spikes showed little slope selectivity (Fig. 3*B*). We further found that the model neuron is capable of burst firing on consecutive up-strokes without an intervening down-stroke (Fig. 3*A*).

Next, we used the reverse correlation technique to examine the features of the input that trigger bursts at different frequencies. We simulated the model neuron receiving a white noise input signal lowpass filtered at different cutoff frequencies. As shown in Figure 3*C*, bursts follow stimulus upstrokes over a wide range of frequencies. Figure 3*D* shows the mean slope of the stimuli preceding bursts at a range of frequencies. The maximal positive slopes (dark red) always precede bursts. Note, that at >10 Hz there is a frequency-dependent delay of bursts up to ~20 msec. This frequency-dependent delay could degrade the temporal precision of slope signaling. The frequency dependence of delay comes about because of the slow membrane properties and in particular because of the slow decay of the dendritic potassium current. There is no delay when the dominant input frequency approximately matches the activation time constant of I_{KS} (τ_{q0} = 200 msec matches 5 Hz). Figure 3*E* shows how the burst delay can be tuned by varying the time constant of activation for I_{KS}. When the activation rate is slow compared with the stimulus frequency, bursts occur with a delay. Thus, the selectivity of bursts for specific stimulus features depends on the tuning of the burst conductances. Taken together, the results of Figures 2 and 3 demonstrate that the burst-mediated mechanism for slope detection is robust for a range of input statistics.

Bidirectional slope signaling

Our findings may be relevant to experimental studies on burst coding in weakly electric fish. Bursts in pyramidal cells of the electrosensory lateral-line lobe detect temporal changes in the surrounding electric field (Gabbiani et al., 1996; Metzner et al., 1998). This is accomplished by two different groups of cells: E-cells that signal the up-stroke and I-cells that signal the down-stroke of field modulations (Bastian, 1981; Shumway and Maler, 1989; Gabbiani et al., 1996). However, the mechanisms underlying this selectivity have been unclear. It is known that E-cells receive excitatory input directly from the electroreceptor afferents, so our previous results provide a reasonable explanation for up-stroke detection solely in terms of the biophysics of bursting. I-cells on the other hand receive indirect inhibitory input via granule cells (Carr et al., 1982), the function of which is to invert the signals from electroreceptor afferents (Fig. 4*C*). Therefore a down-stroke of the external stimulus corresponds to the falling phase of the inhibitory current to the pyramidal cell and thus to the positive slope of the total synaptic drive. We simulated this scenario by inverting the sign of the stimulus to inhibit the soma in the presence of tonic excitatory drive to the dendrites. Figure 4, *A3* and *D*, shows that bursts occur selectively on the down-strokes of the external stimulus. Thus, by inverting the stimulus it becomes possible for bursting cells to detect the negative slope of external stimuli. Therefore within an appropriate network, bursts can be used for bidirectional slope detection.

Burst duration coding

We next asked if bursts only mark the occurrence of slopes or whether they are also capable of signaling the magnitude of the slopes as well. Graded signaling might occur by variations in burst duration (Perkel and Bullock, 1968). Although it is often said that bursts are stereotyped, this is not supported by the evidence (Bair et al., 1994; Reinagel et al., 1999), which reveals considerable variability in the number of spikes per burst (typically two to six). Could the number of spikes per burst and/or burst duration vary with the magnitude of the slope? Figure 5*A* shows that bursts with different number of spikes signal distinct input slopes. Note that this mode of coding is discrete (spikes per burst). This discrete code can be further refined by also considering the time duration of bursts (Fig. 5*D*). Using signal detection theory we quantified how well bursts containing different number of spikes signal the

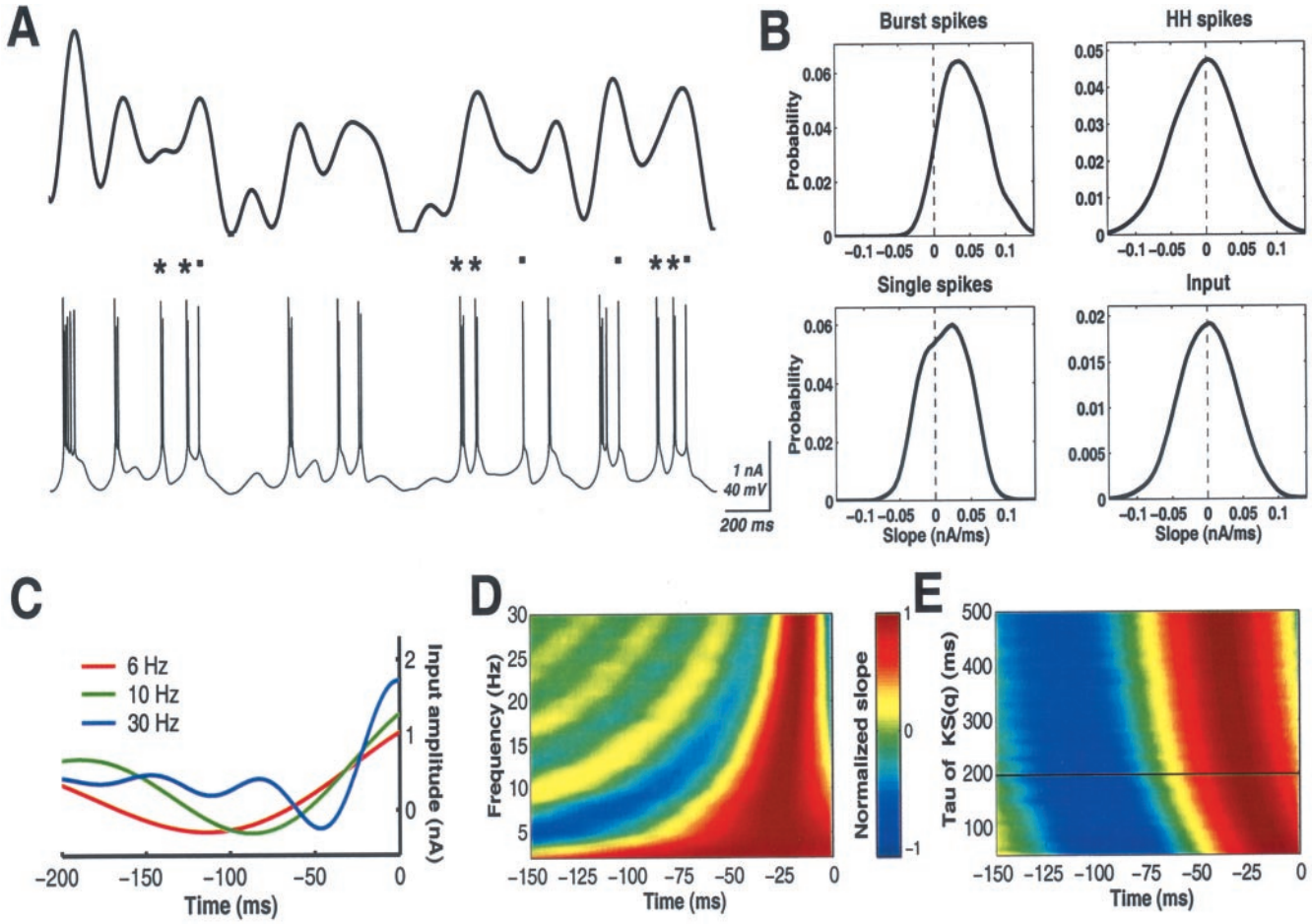

Figure 3. Bursts are triggered on the positive slopes of randomly varying input. *A,* Random input (with cutoff at 5 Hz; mean 1.7; SD 1.0) was applied to the dendrite. Dendritic conductances were adjusted to $g_{NaP} = 0.09$, $g_{KS} = 0.9$ (mS/cm^2) so the model fires single spikes as well (marked with *dots*). The *top trace* shows the random stimulus, and the *bottom trace* shows the membrane potential response. Bursts and single spikes were identified using a 10 msec ISI threshold, which was set based on the ISI distribution. *Asterisks* mark consecutive bursts without an intervening hyperpolarization. *B,* Histogram of input slopes at spike times. Burst spikes occur on positive slopes, whereas single spikes show little slope selectivity. For a tonically spiking model (soma only), the distribution of spikes over different slopes is symmetric for the same signal. *C,* Reverse correlations of the first spikes of bursts with random stimuli. The white noise stimuli had cutoff frequencies of 4, 10, and 30 Hz. Bursts are always preceded by an upstroke. *D,* Reverse correlations of bursts with the derivative of the stimulus. The cutoff frequency of the random stimulus was varied between 2 and 30 Hz. The reverse correlation for each frequency was normalized to the maximum slope (shown with *dark red*). *E,* Same reverse correlations as in *D* with a random stimulus having an 8 Hz cutoff. The factor, τ_{q0}, which scales the activation time constant of the slow potassium conductance, is varied. The standard value is τ_{q0} = 200 msec.

slope and compared this to how well they signal the amplitude of the input. Figure 5*C* shows the ROC curves for slope and amplitude signaling with bursts. This measure shows that for any given false alarm rate, slope is signaled with higher accuracy than amplitude (Fig. 5*C*). To determine whether our conclusions are valid for different types of input we calculated a discriminability index (Gabbiani and Koch, 1998) for inputs with different mean stimulus strengths. The discriminability index is defined as the area under the ROC curve. A value of 0.5 represents chance level, whereas 1 represents perfect discriminability. As shown in Figure 5*D*, burst duration signals the amplitude of the input poorly, but encodes input slope with high fidelity over a large range of stimulus strengths.

Theoretical basis for slope detection and burst duration coding

The slope sensitivity of bursts may be qualitatively understood as follows. A bursting neuron obeys the current balance equation:

$$C_m dV/dt = I_{INPUT} - I_{HH} - I_{BURST} \quad (1)$$

Without active currents (I_{HH} and I_{BURST}) on the right side of the equation, $C_m dV/dt = I_{INPUT}$ dictates that the change of membrane voltage be proportional to the input current. With the addition of spiking currents, I_{HH}, voltage change is translated into a spike frequency code whereby the instantaneous frequency becomes a function of input amplitude (Fig. 6*A*). In a bursting neuron there are additional intrinsic currents (I_{BURST}). At the onset of a burst, I_{BURST} turns on. When these currents dominate ($I_{BURST} > I_{INPUT}$) (Fig. 3*C*), spiking becomes less dependent on input amplitude (Fig. 6*B*). To explain how this leads to slope detection, we base our analysis on the kinetics of the currents defined as I_{BURST}. In our model, I_{BURST} is made up of I_{KS} and I_{NaP}. However, to make our argument more general, we will only use two properties of these currents that are expected to be present in a large class of biophysical mechanisms able to generate intrinsic bursting. (The argument also assumes that the input

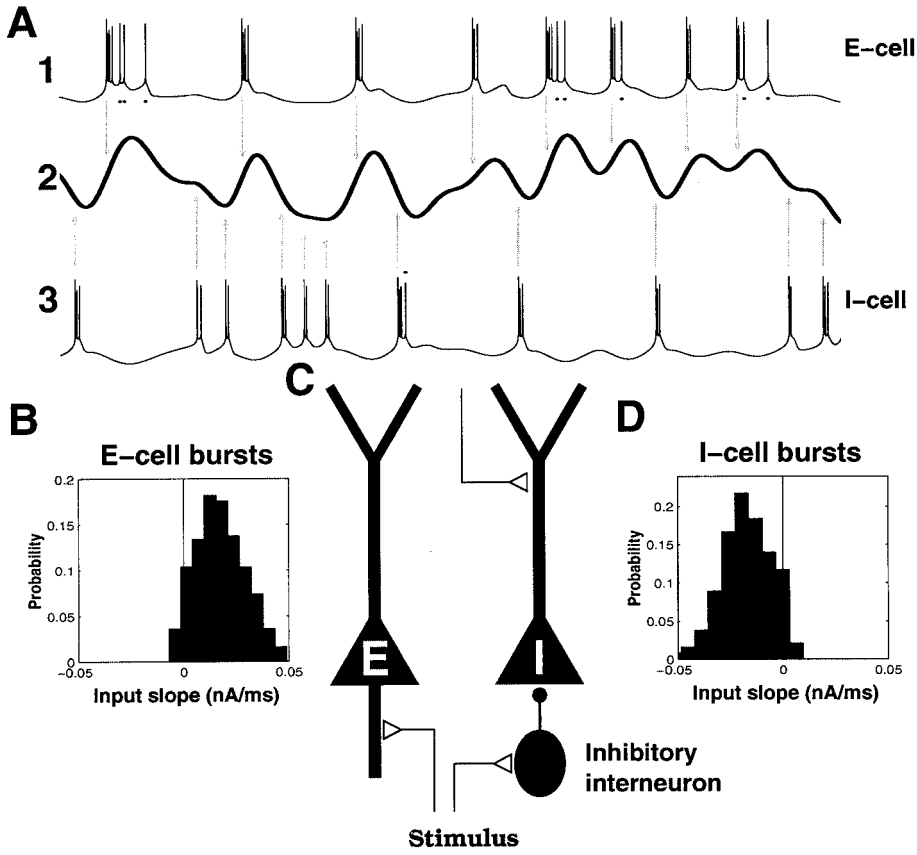

Figure 4. Bidirectional slope detection. *A1*, Upstroke detection. Somatic voltage recording from the E-cell injected with random current (see below) for 3 sec (mean, 1.4; SD, 0.5 nA). Bursts and single spikes were identified using a 10 msec ISI threshold. *Arrows* show that most bursts occur on positive input slopes; isolated spikes (marked with *dots*) can occur on both up- and down-strokes. *A2*, Random input (with cutoff at 5 Hz). *A3*, Down-stroke detection. Simulations with inverted input like at the I-type cells of electric fish. Dendritic compartment receives 2 nA constant input. Somatic input receives the random input with a mean of −3.5 nA and SD of 7.5 nA. *Arrows* show that now bursts occur on negative slopes. *B,* Histogram of input slopes at burst spike times for E-type pyramidal cells. *C,* Structure of the model. Excitation is applied to dendrites of the E-cell. An inhibitory interneuron can invert the signal in which case inhibition is applied to the soma and tonic excitatory drive to the dendrites of the I-cell. The electrosensory lateral line-lobe of the weakly electric fish, which is discussed in Results, has similar anatomical circuits (Carr et al., 1982). *D,* Histogram of input slopes at burst spike times for I-type pyramidal cells.

current is changing much slower than the duration of action potentials.) One property is the fast positive feedback seen in Figure 1*B* and generated in our model by I_{NaP}. The other property is the slower negative feedback shown in Figure 1*C*, which here is generated by I_{KS}. Now consider how I_{BURST} results in positive slope detection. When I_{INPUT} is increasing, it can rapidly activate I_{NaP}, which becomes the dominant current. Then the slow outward current catches up and shuts off the burst. This generates a burst on positive I_{INPUT} slopes. During the downward swing of I_{INPUT}, the slow outward current, I_{KS} is already fully activated while the input current is decreasing, and this makes it unlikely that a burst will be triggered when the slope is negative.

Why should burst duration depend on the magnitude of the slope? Let us consider the condition for burst termination to express burst duration as a function of input parameters. Bursts terminate (Fig. 2*C*) when the net slow currents ($I_{INPUT} - I_{BURST}$) that drive bursting fall below spike threshold, I_{th} (Koch et al., 1995). Recall that $I_{BURST} = I_{KS} - I_{NaP}$. Because I_{NaP} is approximately constant during a burst (Fig. 2*C*), we will use its average value during a burst, A_{NaP}. Assume that I_{INPUT} and I_{KS} change linearly in time during a burst. Then, $I_{INPUT}(t) = A_{INPUT} + S_{INPUT}t$ and $I_{KS}(t) = A_{KS} + S_{KS}t$, where A_{INPUT} and A_{KS} are the values of I_{KS} and I_{INPUT} at the onset of a burst, $t = 0$. S_{INPUT} is the slope of the input current, whereas S_{KS} is the mean slope of I_{KS} during a burst.

Now we consider how the mean activation of I_{KS} depends on the input. I_{KS} is an adaptation current providing proportional negative feedback (Wang, 1998). Hence, A_{KS} tends to track A_{INPUT}. This occurs because I_{KS} is elevated by each spike and decays slowly in time, and the average spike rate over a longer

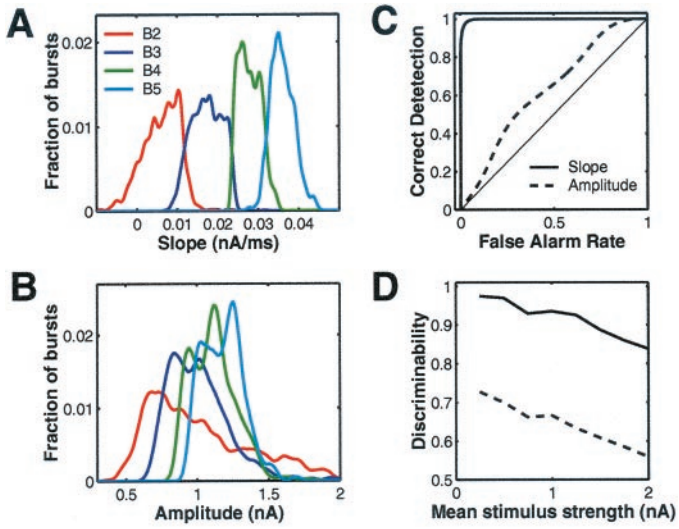

Figure 5. Burst duration codes for input slope. *A,* Distributions of input slopes for bursts of different durations. *B2* represents two spike bursts, *B3* three spike bursts, and so on. Different types of bursts signal distinct slopes with little overlap. *B,* Distributions of input amplitudes for bursts of different durations. The distributions overlap substantially. *C*, ROC curves show the rate of correct detection for a given false alarm rate. Diagonal represents chance level. Curves show discriminability of two and three spike burst distributions in *A* and *B*. *Solid curve,* Slope signaling; *dashed curve,* amplitude signaling. *D,* Discriminability index (area under ROC curve) between two and three spike bursts for slope (*solid*) and amplitude (*dashed*) over a range of random stimuli with different mean strengths.

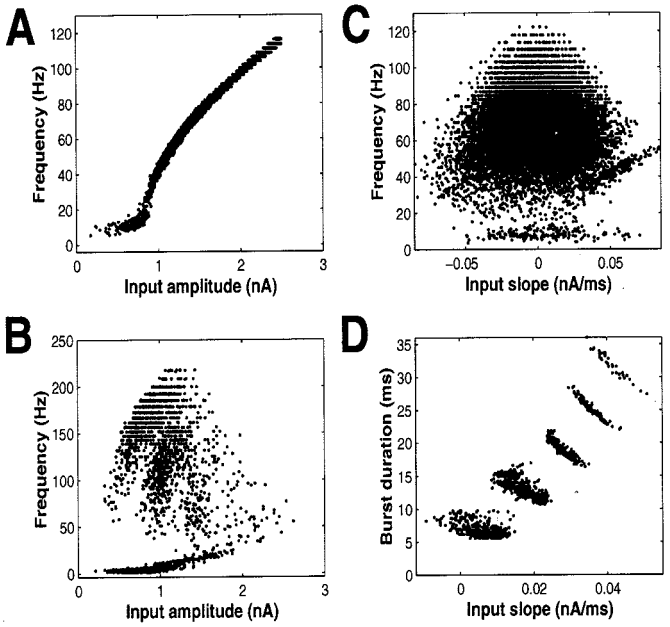

Figure 6. Bursting neurons encode the slope, whereas tonically spiking neurons encode the stimulus amplitude. *A,* Typical frequency input relationship for a tonically spiking neuron (only type 1 Hodgkin–Huxley currents). The stimulus throughout the figure is the same as in Figure 2*a*. The instantaneous frequency is shown, which was calculated as the reciprocal of an interspike interval. *B,* Instantaneous frequency input relationship for the bursting model shows no clear amplitude coding. *C,* For a tonically spiking neuron, frequency does not encode input slope. *D,* Burst duration is a function of input slope. Steps are caused by the additions of further spikes to bursts; each cluster contains a given spike count.

interval is proportional to the mean input. Thus, in this regime, $A_{KS} \sim \kappa A_{INPUT}$. From our simulations we found that $\kappa = 0.9$ (see Fig. 8*B*), but this constant is expected to change with the kinetics of I_{KS} as well as the properties of the input.

Recall that bursts terminate ($t = T_{BURST}$) when $I_{INPUT} - I_{BURST}$ falls below I_{th}. This can be expressed as $I_{INPUT} + I_{NaP} - I_{KS} \simeq A_{INPUT}(1 - \kappa) + A_{NaP} + (S_{INPUT} - S_{KS})T_{BURST} \simeq I_{th}$. From this we can now express burst duration:

$$T_{BURST} \simeq \frac{(1 - \kappa)A_{INPUT} + A_{NaP} - I_{th}}{(S_{KS} - S_{INPUT})} \quad (2)$$

This equation can also be obtained by a fast–slow variable mathematical analysis of burst generation (see Appendix). This relationship shows that burst duration depends only weakly on the input amplitude, A_{INPUT}. By contrast, burst duration increases strongly with input slope, S_{INPUT}. This relationship between burst duration, T_{BURST}, and input slope, S_{INPUT}, captures the mean simulation data (Fig. 6*D*). Note that Figure 6*D* also shows clusters representing bursts of a given spike count, which is not accounted for by Equation 2. Thus, for the kinds of burst we have analyzed we are able to provide an explanation for why bursts have positive slope selectivity and why burst duration varies with the magnitude of the slope.

Slope detection with other bursting neurons

In our previous simulations we showed that for a particular type of bursting mechanism involving I_{NaP} and I_{KS}, both the timing of bursts as well as the burst duration depend on the input slope. As the analysis in the previous section suggests, this property of bursts is more general. Figure 7*A* shows that similar burst coding occurs when the bursting mechanism involves high-threshold calcium and calcium-dependent potassium currents (Wang, 1998).

Another class of neurons, the chattering cells located in the superficial layers of visual cortex, can fire brief bursts at very high frequencies (Gray and McCormick, 1996). These bursts are thought to be generated by an interplay between sodium and potassium conductances (Wang, 1999; Brumberg et al., 2000). We used a previously published model of chattering cells (Wang, 1999) to examine the coding properties of bursts. In agreement with our previous findings, the chattering neuron model also fired bursts at the rising edges of the stimulus with a duration proportional the input slope (Fig. 7*B*).

DISCUSSION

We have examined the input–output relationship of a class of bursting neurons using a standard model of bursting pyramidal cells. We first examined the timing of bursts during sinusoidal current injections and found that bursts tend to occur on the rising edge of the input (Fig. 2*B*) at low frequencies (1–10 Hz) as reported previously (Kamondi et al., 1998; Smith et al., 2000). Next, we examined this slope detection property with more naturalistic current injections. Our simulations showed that bursts are preferentially triggered by positive input slopes (Fig. 3). Single spikes on the other hand showed no slope selectivity at these frequencies. Using random inputs with different, low-frequency components, we found that bursts occur at a small delay (up to 20 msec) with respect to the maximal stimulus slope at higher frequencies (>10 Hz). The preferred range of frequency selectivity is primarily determined by the activation time constant of the slow potassium conductance responsible for terminating bursts. Therefore the burst-mediated mechanism for slope detection is robust within a reasonable range of input statistics.

Is there experimental evidence indicating that bursts signal slope? Studies of weakly electric fish reported that pyramidal neurons detect temporal changes (slope) in the self-generated electric fields (Bastian, 1981; Heiligenberg, 1991). Recent work on these pyramidal cells has shown that bursts are particularly reliable at signaling stimulus slope (Gabbiani et al., 1996; Metzner et al., 1998). However, the origin of this selectivity has been unclear. Gabbiani et al. (1996) pointed out that this selectivity could not be explained with a simple integrate-and-fire mechanism based on their recordings of the membrane potential. Our results show that slope selectivity can result directly from the biophysics of a burst generation process. Interestingly, slope detection is accomplished by two different groups of cells in the electrosensory lateral-line lobe (Fig. 4*C*): E-cells that signal the rising and I-cells that signal the falling edge of external stimuli (Bastian, 1981; Shumway and Maler, 1989; Gabbiani et al., 1996). Whereas E-cells receive excitatory input directly from the electroreceptor afferents, I-cells receive indirect stimulus input via inhibitory granule cells (Carr et al., 1982; Berman and Maler, 1998). Using this principle, we showed that by inverting the stimulus to inhibit the neuron while tonically depolarizing it, bursts occur on the negative slopes. Therefore the example of the electric fish shows how slope detection by bursts can be adapted for bidirectional signaling (Fig. 4) and used in a behaviorally important computation (Maler, 1996; Gabbiani and Metzner, 1999).

We have also found several other reports in the literature supporting the notion of slope detection by bursts. A particularly clear example is provided by relay cells of the thalamus. When tonically hyperpolarized, these cells generate bursts that occur

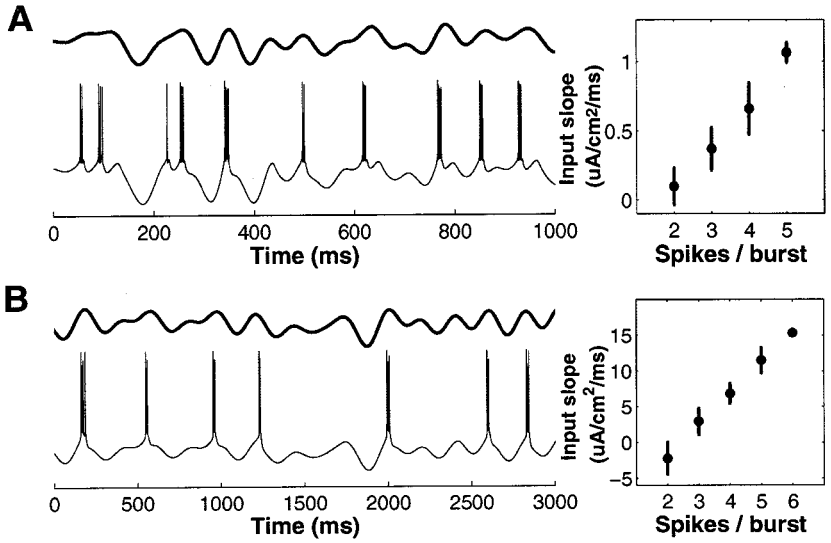

Figure 7. Other bursters also signal slope. *A,* Slope detection in a neuron model with a calcium-dependent bursting mechanism. The stimulus is random up to a cutoff frequency of 5 Hz (mean 0.5; SD 1.1 $\mu A/cm^2$). The *panel* on the *right* shows the derivative of the stimulus at the onset of the burst as a function of burst duration. Error bars indicate SD. *B,* Chattering neuron model. Note that chattering cells fire faster bursts and recover more rapidly from after-hyperpolarization, and therefore we used random input with 15 Hz frequency cutoff (mean 2.2; SD 6.5 $\mu A/cm^2$).

exclusively on the rising edge of sinusoidal input current both *in vitro* in slice (Smith et al., 2000) as well as *in vivo* in anesthetized cats (Guido et al., 1992). An additional example of slope detection by bursts occurs in the lobster stomatogastric nervous system, where in its bursting mode, a sensory neuron encodes the positive slope of muscle stretch (J. T. Birmingham, personal communication).

Diversity of bursting mechanisms

While burst firing can result from a multiplicity of ionic mechanisms there are key properties that define a large class of bursting neurons (Rinzel, 1987; Wang and Rinzel, 1995). First, bursts can outlast the input that triggered them (Fig. 1*B*). Second, because they are strongly adapting, firing will stop abruptly even if input is sustained (Fig. 1*C*). These properties of bursts result from ionic conductances that provide fast positive feedback to boost firing rates and slower negative feedback to make bursts strongly adapting. We define any set of current or currents that accomplish this as the burst currents, I_{BURST}. This can be thought of a module of conductances that perform in a functionally similar manner.

Although we use the I_{NaP} and I_{KS} currents to create a "burst module", other conductances can be also used that work together in a similar way. For instance, there is evidence that a high-threshold calcium current, I_{CaL}, and calcium-dependent potassium current, I_{AHP}, generate bursting (Fig. 7*A*) in pyramidal cells (Wong et al., 1979; Golding et al., 1999; Magee and Carruth, 1999; Williams and Stuart, 1999). Our results show that these bursting currents can make neurons more sensitive to the slope of the input current than its amplitude (Figs. 2, 3, 7). When I_{BURST} has the functional form defined above, we showed that both the timing as well as the duration of bursts will depend on input slope.

Other classes of neurons can have different types of bursting mechanisms. For instance, low-threshold bursts in the thalamus require a preceding hyperpolarization to deinactivate T-type calcium channels (Jahnsen and Llinás, 1984; Zhan et al., 1999), and the inactivation of these channels is primarily responsible for burst termination (Wang et al., 1991). Therefore, although our arguments still suggest that the timing of bursts will be controlled by input slope, as observed previously (Guido et al., 1992; Smith et al., 2000), the duration of bursts may encode other stimulus variables such as the length of preburst silent period. Because neurons are equipped with a rich repertoire of ionic mechanisms that result in bursting (Epstein and Marder, 1990; Wang and Rinzel, 1995), it will be interesting to compare the rules by which different types of bursters transform their inputs.

Spatial control of bursting

Although our results clearly show that bursts can signal slope, the temporal aspects of input may not be the only determinants of whether a burst occurs. Indeed, there is evidence that burst generation in pyramidal cells can additionally be gated by top-down, feedback signals from higher centers that terminate on the distal apical dendrites (Cauller et al., 1998; Larkum et al., 1999; Bastian and Nguyenkim 2001). Therefore, it is possible that cells that fire bursts in response to the temporal properties of the input (slope) may only do so when a certain spatial configuration of inputs is present (Larkum et al., 1999; Bastian and Nguyenkim, 2001). According to this notion, the propensity to burst is enhanced by excitatory input onto the distal dendrites, but whether a burst will occur will depend on the temporal properties of more proximal inputs. In fact, the models we analyzed incorporate burst generating conductances that are located in the dendritic compartment. Although this is not strictly necessary for slope-detection, it can lay the ground for further work to understand the interplay between spatial and temporal factors in the control of bursting (Kepecs and Wang, 2000).

Burst duration coding

Our results also revealed a new aspect of burst signaling: burst duration coding. We found that the differences in burst duration, specifically the spike count (Fig. 5*A*) and the time duration (Fig. 6*D*) signal the magnitude of the input slope in a graded manner. Burst duration is a potentially significant neural code because it allows graded information to be transmitted in <20 msec. For example, if action potential frequency is 250 Hz during a burst, bursts containing 2–6 spikes would have durations ranging from 4 to 20 msec (Guido et al., 1992). This gradation is only possible because firing rate has been pushed to its upper limit because of the bursting mechanism. Because multiple spikes can occur in a short period, individual cells can rapidly provide statistically strong information about the input. Given this power of burst duration coding, it will be important to investigate its occurrence in different types of neurons. There is some indication that it occurs in complex cells of the visual cortex, where the number of

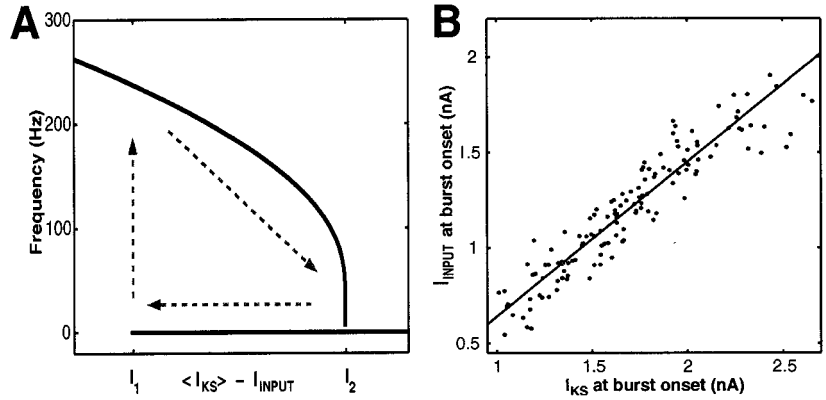

Figure 8. Determinants of bursting. *A,* Bifurcation diagram of the model showing how spike frequency changes as a function of input. Bursting starts at I_1 and ends at a homoclinic bifurcation at I_2. *Arrows* mark the evolution (decrease) of frequency during bursts and the quiescent period in between bursts. *B,* Mean I_{KS} tracks I_{INPUT}. *Dots* show data points from individual bursts. Both the input current as well as the current from the slow potassium channels were measured at the onset of bursting. The best fit line has a slope of 0.9.

spikes per burst is modulated by stimulus orientation (DeBusk et al., 1997) and preliminary evidence shows burst duration coding in the lateral geniculate nucleus (Kepecs et al., 2001).

We have addressed a fundamental aspect of neuronal signaling, how input to a neuron is transformed into an output spike pattern. The standard view of this process is that stimulus intensity is transformed into a spike frequency code (Adrian, 1932; Shadlen and Newsome, 1994). At the level of individual neurons this intensity-to-frequency transduction relies on the spiking currents, as described by Hodgkin and Huxley (1952). These spiking currents (I_{HH}) are present in most neurons and generate action potentials with a frequency proportional to the magnitude of current input. The spiking process can be captured by the integrate-and-fire model (Lapicque, 1907; Tuckwell, 1988; Kistler et al., 1997), which has provided a useful framework to understand the response properties of many types of neurons (Reich et al., 1997; Shadlen and Newsome, 1998; Binder et al., 1999).

Our study emphasizes that as neurons are endowed with a richer repertoire of voltage-gated conductances, their input–output relationship becomes more complex, and their computational capabilities change. In particular, these intrinsic conductances can determine whether a cell will burst or fire regular spike trains. As we show here, some bursting neurons can perform a differentiate and burst computation that is fundamentally different from the integrate and fire function of simple spiking cells. The ability of these bursting cells to signal slope (Fig. 6) can be used to make behaviorally important computations and may underlie a burst duration code useful for rapid information transfer.

APPENDIX

Bursts can be analyzed mathematically with the "fast–slow variable dissection method" (Rinzel, 1987; Rinzel and Ermentrout, 1989). The method is based on the idea that different components of bursting act on very different time scales and can therefore be analyzed separately. In our case, the potassium current I_{KS} and the input current I_{INPUT} vary much more slowly than the spike-generating dynamics. The slow and fast membrane processes can be therefore separated by first considering how the behavior of the fast spiking subsystem depends on the slow, $I(t) = I_{KS} - I_{INPUT}$, as if the latter were a fixed parameter. In a second step, the slow time course of $I(t)$ is considered, which then predicts how the burst firing pattern evolves in time. This analysis clarifies the assumptions made in the previous derivation and in particular eliminates the need to assume that bursts terminate at a given current threshold, I_{th}.

Figure 8*A* shows a bifurcation diagram (Kepecs and Wang, 2000), where the fast system is represented by the neuronal firing frequency as a function of $I = I_{KS} - I_{INPUT}$. The dynamics of the slow system is represented by the arrows. At a critical value, I_1, bursting commences with maximal frequency. During a burst, I_{KS} increases slowly but at a higher rate than I_{INPUT}, so that I increases, and the firing frequency monotonically decreases. Using a linear approximation, we can express this relationship as $f(I) = f_0 - \frac{I - I_1}{I_2 - I_1} f_0$, where $f_0 = f(I_1)$ is the frequency at the onset of bursting. At the beginning of the burst, $t = 0$ and $I = I_1$. From Figure 2*C* we observe that I_{KS} increases in an approximately linear manner during a burst: $I_{KS} = A_{KS} + S_{KS}t$, and we rewrite the input current similarly as $I_{INPUT} = A_{INPUT} + S_{INPUT}t$. Now, $I_1 = A_{KS} - A_{INPUT}$. As an adaptation current the mean I_{KS} tends to track the mean input (Wang, 1998), $A_{KS} = C_{KS} + \kappa A_{INPUT}$. From our simulations we find that $\kappa = 0.9$ (Fig. 8*B*). Thus, $I_1 = (\kappa - 1)A_{INPUT} + C_{KS}$. We can now write $I(t) = I_1 + (S_{KS} - S_{INPUT})t$. Using these relationships we can write the time evolution of frequency as $f(t) = f_0 \left[1 - \frac{(S_{KS} - S_{INPUT})t}{I_2 - I_1}\right]$. A burst terminates ($t = T$) when its frequency goes to zero: $f(T) = 0$. From these we can express burst duration, $T = \frac{I_2 - I_1}{S_{KS} - S_{INPUT}} = \frac{\text{const}_1 + (1 - \kappa)A_{INPUT}}{\text{const}_2 - S_{INPUT}}$, with $\text{const}_1 = I_2 - C_{KS}$ and $\text{const}_2 = S_{KS}$. Thus burst duration increases nonlinearly and dramatically with input slope, S_{INPUT}, whereas its dependence on the input amplitude, A_{INPUT}, is weak.

Our argument still holds if the dependence of the firing rate f on I is not linear, e.g., is instead a quadratic function near the saddle node bifurcation at I_2 (Rinzel, 1987; Rinzel and Ermentrout, 1989).

REFERENCES

Adrian E (1932) The mechanism of nervous action: electrical studies of the neurone. Philadelphia, PA: University of Pennsylvania.

Azouz R, Jensen M, Yaari Y (1996) Ionic basis of spike after-depolarization and burst generation in adult rat hippocampal CA1 pyramidal cells. J Physiol (Lond) 492:211–223.

Bair W, Koch C, Newsome W, Britten K (1994) Power spectrum analysis of bursting cells in area MT in the behaving monkey. J Neurosci 14:2870–2892.

Barker J, Gainer H (1975) Studies on bursting pacemaker potential activity in molluscan neurons I. membrane properties and ionic contributions. Brain Res 84:461–477.

Bastian J (1981) Electrolocation II: The effects of moving objects and other electrical stimuli on the activities of two categories of posterior lateral line lobe cells in *Apteronotus albifrons*. J Comp Physiol [A] 144:481–494.

Bastian J, Nguyenkim J (2001) Dendritic modulation of burst-like firing in sensory neurons. J Neurophysiol 85:10–22.

Berman N, Maler L (1998) Inhibition evoked from primary afferents in the electrosensory lateral line lobe of the weakly electric fish. J Neurophysiol 80:3173–3196.
Binder M, Poliakov A, Powers R (1999) . Functional identification of the input-output transforms of mammalian motoneurones. J Physiol (Paris) 93:29–42.
Brumberg J, Nowak L, McCormick D (2000) Ionic mechanisms underlying repetitive high-frequency burst firing in supragranular cortical neurons. J Neurosci 20:4829–4843.
Carr C, Maler L, Sas E (1982) Peripheral organization and central projections of the electrosensory nerves in gymnotoid fish. J Comp Neurol 211:139–153.
Cattaneo A, Maffei L, Morrone C (1981a) Patterns in the discharge of simple and complex visual cortical cells. Proc R Soc Lond B Biol Sci 212:279–297.
Cattaneo A, Maffei L, Morrone C (1981b) Two firing patterns in the discharge of complex cells encoding different attributes of the visual stimulus. Exp Brain Res 43:115–118.
Cauller L, Clancy B, Connors B (1998) Backward cortical projections to primary somatosensory cortex in rats extend long horizontal axons in layer I. J Comp Neurol 390:297–310.
DeBusk B, DeBruyn E, Snider R, Kabara J, Bonds A (1997) Stimulus-dependent modulation of spike burst length in cat striate cortical cell. J Neurophysiol 78:199–213.
Doedel E (1981) AUTO: A program for the automatic bifurcation and analysis of autonomous systems. Cong Num 30:265–284.
Doiron B, Longtin A, Turner R, Maler L (2001) Model of gamma frequency burst discharge generated by conditional backpropagation. J Neurophysiol 86:1523–1545.
Eisen J, Marder E (1982) Mechanisms underlying pattern generation in lobster stomatogastric ganglion as determined by selective inactivation of identified neurons. III. synaptic connections of electrically coupled pyloric neurons. J Neurophysiol 48:1392–1415.
Epstein I, Marder E (1990) Multiple modes of a conditional neural oscillator. Biol Cybern 63:25–34.
Ermentrout GE (2002) Simulating, analyzing, and animating dynamical systems: a guide to XPPAUT for researchers and students. Philadelphia: Society for Industrial and Applied Mathematics.
Gabbiani F, Koch C (1998) Methods in neuronal modeling, Chapter principles of spike train analysis, pp 313–360. Cambridge, MA: MIT.
Gabbiani F, Metzner W (1999) Encoding and processing of sensory information in neuronal spike trains. J Exp Biol 202:1267–1279.
Gabbiani F, Metzner W, Wessel R, Koch C (1996) From stimulus encoding to feature extraction in weakly electric fish. Nature 386:564–567.
Gariano R, Groves P (1988) Burst firing induced in midbrain dopamine neurons by stimulation of the medial prefrontal and anterior cingulate cortices. Brain Res 462:194–198.
Golding N, Jung H, Mickus T, Spruston N (1999) Dendritic calcium spike initiation and repolarization are controlled by distinct potassium channel subtypes in CA1 pyramidal neurons. J Neurosci 19:8789–8798.
Gray C, McCormick D (1996) Chattering cells: superficial pyramidal neurons contributing to the generation of synchronous oscillations in the visual cortex. Science 274:109–113.
Green D, Swets J (1966) Signal detection theory and psychophysics. New York: Wiley.
Guido W, Lu S, Sherman S (1992) Relative contributions of burst and tonic responses to the receptive field properties of lateral geniculate neurons in the cat. J Neurophysiol 68:2199–2211.
Harris K, Hirase H, Leinekugel X, Henze D, Buzsáki G (2001) Temporal interaction between single spikes and complex spike bursts in hippocampal pyramidal cells. Neuron 32:141–149.
Heiligenberg W (1991) Neural nets in electric fish. Cambridge, MA: MIT.
Hodgkin A (1948) The local changes associated with repetitive action in a nonmedullated axon. J Physiol (Lond) 107:165–181.
Hodgkin A, Huxley A (1952) A quantitative description of membrane current and its application to conduction and excitation in nerve. J Physiol (Lond) 117:500–544.
Hoffman A, Magee J, Colbert C, Johnston D (1997) K^+ channel regulation of signal propagation in dendrites of hippocampal pyramidal neurons. Nature 387:869–875.
Huerta P, Lisman J (1995) Bidirectional synaptic plasticity induced by a single burst during cholinergic theta oscillation in CA1 in vitro. Neuron 15:1053–1063.
Jahnsen H, Llinás R (1984) Electrophysiological properties of guinea pig thalamic neurones: an *in vitro* study. J Physiol (Lond) 349:205–226.
Kamondi A, Acsády L, Wang X-J, Buzsáki G (1998) Theta oscillations in somata and dendrites of hippocampal pyramidal cells in vivo: activity-dependent phase-precession of action potentials. Hippocampus 8:244–260.
Kandel E, Spencer W (1961) Electrophysiology of hippocampal neurons. II. After-potentials and repetitive firing. J Neurophysiol 24:243–259.
Kepecs A, Wang X-J (2000) Analysis of complex bursting in cortical pyramidal neuron models. Neurocomputing 32:181–187.
Kepecs A, Sherman S, Lisman J (2001) Burst duration coding in cat LGN. Soc Neurosci Abstr 31:13295.
King W, Lisberger S, Fuchs A (1976) Responses of fibers in medial longitudinal fasciculus (MLF) of alert monkeys during horizontal and vertical conjugate eye movements evoked by vestibular or visual stimuli. J Neurophysiol 39:1135–1149.
Kistler W, Gerstner W, van Hemmen J (1997) Reduction of Hodgkin–Huxley equations to a threshold model. Neural Comput 9:1069–1100.
Koch C, Bernander O, Douglas R (1995) Do neurons have a voltage or a current threshold for action potential initiation? J Comp Neurosci 2:63–82.
Lapicque L (1907) Recherches quantitatives sur l'excitation electrique des nerfs traitee comme une polarization. J Physiol Pathol Gen 9:620–635.
Larkum M, Zhu J, Sakmann B (1999) A new cellular mechanism for coupling input arriving at different cortical layers. Nature 398:338–341.
Lisman J (1997) Bursts as units of neural information. Trends Neurosci 20:38–41.
Livingstone M, Freeman D, Hubel D (1996) Visual responses in V1 of freely viewing monkeys. Cold Spring Harb Symp Quant Biol 61:27–37.
Magee J, Carruth M (1999) Dendritic voltage-gated ion channels regulate the action potential firing mode of hippocampal CA1 pyramidal neurons. J Neurophysiol 82:1895–1901.
Mainen Z, Sejnowski T (1996) Influence of dendritic structure on firing pattern in model neocortical neurons. Nature 382:363–366.
Maler L (1996) Train signals for electric fish. Nature 384:517–518.
Martinez-Conde S, Macknik S, Hubel D (2000) Microsaccadic eye movements and firing of single cells in the striate cortex of macaque monkeys. Nat Neurosci 3:251–258.
Matveev V, Wang X-J (2000) Differential short-term synaptic plasticity and transmission of complex spike trains: to depress or to facilitate? Cereb Cortex 10:1143–1153.
Metzner W, Koch C, Wessel R, Gabbiani F (1998) Feature extraction by burst-like spike patterns in multiple sensory maps. J Neurosci 18:2283–2300.
Miles R, Traub R, Wong R (1988) Spread of synchronous firing in longitudinal slices from the CA3 region of the hippocampus. J Neurophysiol 60:1481–1496.
Molden S, Fyhn M, Hollup S, Moser M-B, Moser E (2001) Place correlates of complex spikes in CA1 pyramidal cells. Soc Neurosci Abstr 32:643–644.
Otto T, Eichenbaum H, Wiener S, Wible C (1991) Learning-related patterns of CA1 spike trains parallel stimulation parameters optimal for inducing hippocampal long-term potentiation. Hippocampus 1:181–192.
Pavlides C, Greenstein Y, Grudman M, Winson J (1988) Long-term potentiation in the dentate gyrus is induced preferentially on the positive phase of theta-rhythm. Brain Res 439:383–387.
Perkel D, Bullock T (1968) Neural coding. Neurosci Res Prog Bull 6:221–348.
Pike F, Meredith R, Olding A, Paulsen O (1999) Rapid report: postsynaptic bursting is essential for "Hebbian" induction of associative long-term potentiation at excitatory synapses in rat hippocampus. J Physiol (Lond) 518:571–576.
Pinsky P, Rinzel J (1994) Intrinsic and network rhythmogenesis in a reduced Traub model for CA3 neurons. J Comp Neurosci 1:39–60.
Ramcharan E, Gnadt J, Sherman S (2000) Burst and tonic firing in thalamic cells of unanesthetized, behaving monkeys. Vis Neurosci 17:55–62.
Reich D, Victor J, Kaplan E (1997) Response variability and timing precision of neuronal spike trains in vivo. J Neurophysiol 77:2836.
Reinagel P, Godwin D, Sherman S, Koch C (1999) Encoding of visual information by LGN bursts. J Neurophysiol 81:2558–2569.
Rhodes P, Gray C (1994) Simulations of intrinsically bursting neocortical neurons. Neural Comput 6:1086–1110.
Rinzel J (1987) Proceedings of the International Congress of Mathematicians. A formal classification of bursting mechanisms in excitable cells, pp 1578–1594. Providence, RI: American Mathematicians Society.
Rinzel J, Ermentrout G (1989) Methods in neuronal modeling, Chapter analysis of neural excitability and oscillations, pp 135–170. Cambridge, MA: MIT.
Shadlen M, Newsome W (1994) Noise, neural codes and cortical organization. Curr Opin Neurobiol 4:569–579.
Shadlen M, Newsome W (1998) The variable discharge of cortical neurons: implications for connectivity, computation and information coding. J Neurosci 18:3870–3896.
Sherman S (2001) Tonic and burst firing: dual modes of thalamocortical relay. Trends Neurosci 24:122–126.
Shumway C, Maler L (1989) GABAergic inhibition shapes temporal and spatial response properties of pyramidal cells in the electrosensory lateral line lobe of gymnotiform fish. J Comp Physiol [A] 164:391–407.
Silva L, Amitai Y, Connors B (1991) Intrinsic oscillations of neocortex generated by layer 5 pyramidal neurons. Science 251:432–435.
Smith G, Cox C, Sherman S, Rinzel J (2000) Fourier analysis of sinu-

soidally driven thalamocortical relay neurons and a minimal integrate-and-fire-or-burst model. J Neurophysiol 83:588–610.
Thomas M, Watabe A, Moody T, Makhinson M, O'Dell T (1998) Postsynaptic complex spike bursting enables the induction of LTP by theta frequency synaptic stimulation. J Neurosci 18:7118–7126.
Traub R, Wong R, Miles R, Michelson H (1991) A model of a CA3 hippocampal pyramidal neuron incorporating voltage-clamp data on intrinsic conductances. J Neurophysiol 66:635–650.
Tuckwell H (1988) Introduction to theoretical neurobiology. Cambridge, UK: Cambridge UP.
Turner R, Maler L, Deerinck T, Levinson S, Ellisman M (1994) TTX-sensitive dendritic sodium channels underlie oscillatory discharge in a vertebrate sensory neuron. J Neurosci 14:6453–6471.
Wang X-J (1998) Calcium coding and adaptive temporal computation in cortical pyramidal neurons. J Neurophysiol 79:1549–1566.
Wang X-J (1999) Fast burst firing and short-term synaptic plasticity: a model of neocortical chatterning neurons. Neuroscience 89:347–362.
Wang X-J, Buzsáki G (1996) Gamma oscillation by synaptic inhibition in a hippocampal interneuronal network model. J Neurosci 16:6402–6413.
Wang X-J, Rinzel J (1995) Oscillatory and bursting properties of neurons. In: Handbook of brain theory and neural networks, pp 686–691. Boston: MIT.
Wang X-J, Rinzel J, Rogawski M (1991) A model of the T-type calcium current and the low-threshold spike in thalamic neurons. J Neurophysiol 66:839–850.
Williams S, Stuart G (1999) Mechanisms and consequences of action potential burst firing in rat neocortical pyramidal neurons. J Physiol (Lond) 521:467–482.
Wong R, Prince D, Basbaum A (1979) Intradendritic recordings from hippocampal neurons. Proc Natl Acad Sci USA 76:986–990.
Zhan X, Cox C, Rinzel J, Sherman S (1999) Current clamp and modeling studies of low-threshold calcium spikes in cells of the cat's lateral geniculate nucleus. J Neurophysiol 81:2360–2373.